Vol. 5 No.3 July 2022

Journal of Networking and Communication Systems

Received 29 April, Revised 15 July, Accepted 20 July

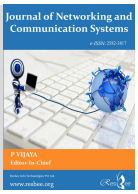

EHSCO-Deep Residual Network: Elephant Herding Sine Cosine Optimization-based Deep Residual network for Diabetic Retinopathy Detection

Komal S. Gandle

Department of Information Technology

Government College of Engineering, Aurangabad, Maharashtra, India.

Abstract: Diabetic retinopathy (DR) is a widespread problem of diabetes and is one of the main causes of loss of sight in the dynamic population. Several complications of DR can be prevented by timely behavior and blood glucose control. In this paper, the Elephant Herding Sine Cosine Optimization-based Deep Residual network (EHSCO-based Deep Residual Network) is developed for the DR detection. Here, pre-processing is performed for the input image using the grayscale conversion and Type 2 Fuzzy and Cuckoo Search-Based Filter (T2FCS). After that, the optic disc detection is carried out using Sparse Fuzzy C-Means clustering (Sparse FCM), whereas the blood vessel detection is performed using Morphological Top-Hat transform for the pre-processed input image. Besides, feature extraction is performed to extract the features, such as Texton, Walsh Hadamard transform, mean, variance, entropy and kurtosis. Finally, the extracted features are given to the detection module, which is carried out based on Deep Residual Network classifier. In addition, the employed classifier is trained by the developed EHSCO optimization algorithm. Here, the developed EHSCO-based Deep Residual Network is the combination of Elephant Herding Optimization (EHO) and Sine Cosine Algorithm (SCA). Besides, the developed DR detection technique obtained efficient performance in terms of maximum True Positive Rate (TPR) with 0.963, maximal True Negative Rate (TNR) with 0.959, and higher accuracy with 0.956 with respect to DIARETDB0 dataset respectively.

Keywords: Diabetic Retinopathy, Deep Residual Network, Elephant Herding Optimization, Walsh Hadamard Transform, Sine Cosine Algorithm.

1. Introduction

Diabetic retinopathy (DR), one of the most widespread retinal disorders, is a common problem of diabetes and is the leading reason of blindness in humans. Because the disease is a progressive procedure, medical professionals recommend that diabetics have to be screened at least twice a year to timely diagnose signs of the disease. In current clinical analysis, detection relies primarily on an ophthalmologist analyzing a colored fundus image and then assessing the condition of the patient. This detection is tedious and time consuming, which increases the number of errors. In addition, due to the large number of diabetic patients and lack of medical resources in some areas, many DR patients cannot be diagnosed and treated in a timely manner, resulting in the loss of best treatment options and ultimately can lead to irreversible loss of vision and blindness [5]. The main cause of DR is poor control of blood glucose levels, and the majority of diabetics do not choose a fundamental analysis of DR because it is a time-consuming procedure [6]. Early prediction of DR can play an important role in preventing vision loss. In addition, structural changes caused by the vascular system may provide physical signs of illness. Therefore, experts advise patients to undergo an annual retinal screening test with an expanded eye examination [9] [4].

According to the latest report of the World Health Organization (WHO) [17], at least 2.2 billion people across the world have blindness or vision problems. More importantly, at least one billion people have eye conditions that were preventable or still in need of treatment [19]. The number of people with eye disease is expected to increase dramatically in later years, primarily due to aging, behavioral and lifestyle changes, and the increasing urbanization of the population [18]. Visual loss or severe eye disease due to the onset and progression of DR can normally be avoided with early detection and timely treatment. Meanwhile, the process of detecting the DR is very difficult because there are no obvious signs or symptoms until DR reaches the stage of low vision. In addition, ignorance of DR symptoms

https://doi.org/10.46253/jnacs.v5i3.a3

among the general public is another important factor in early detection. These factors make DR one of the leading causes of blindness worldwide [15]. Hence, early identification of DR is very important and is made possible by ophthalmoscopic investigations during regular physical eye examinations. During an ophthalmoscopic examination (also known as a funduscopy) an ophthalmologist looks into the interior surface of the eye using an ophthalmoscope to identify pathognomonic indications of DR such as hemorrhages (HMs), soft/hard exudates (EXs), and microaneurysms (MAs) [16] [7].

Computer-Aided Diagnosis (CAD) systems can play an important role in the early detection of DR. Recent advances in fundus photography [6] allow CAD systems to detect and identify the structure of interest in a semi-automatic or fully automated manner [13] [14], making it easy to distinguish between normal and DR fundus images. Therefore, the CAD systems can be used during the pre-screening phases to address the following issues, like limited accessibility of ophthalmic medical professionals and an increasing number of DR patients, intrinsic variability in diagnostic actions and quality across communities, substantial social and personal burden of blindness and low vision [7]. Moreover, Deep learning techniques show excellent performance in identifying DRs and offer a high level of accuracy that sets them apart from other models. Undoubtedly, deep learning can reveal hidden elements of images that medical professionals never see. Convolutional neural networks (CNNs) are the most widely used deep learning approach in healthcare systems because of their capability in extracting the features and training in discriminating among multi-classes [10]. For some medical datasets, the transfer learning approach also facilitated rapid and reliable retraining of deep neural networks [11] [12] [4].

This research is developed by employing the proposed EHSCO algorithm for the DR detection. The proposed approach consists of various stages, such as pre-processing, object disc detection, blood vessel segmentation, feature extraction, and DR detection. Initially, the input image is pre-processed, and then fed to the object disc detection stage where the process is carried out using Sparse FCM. The pre-processed image is subjected to the blood vessel segmentation stage for segmenting the blood vessels using the morphological top-hat transform. After that, the feature extraction process is performed based from the gray scale image, optic disc segmented image, blood vessel segmented image, such that the Walsh Hadamard transform, TEXTON features, mean, variance, entropy and kurtosis are extracted for further processing. Furthermore, the number of features extracted from the feature extraction phase is fed as an input to Deep residual network classifier, where the classifier is trained using the developed EHSCO algorithm. However, the proposed EHSCO is derived by the integration of EHO with SCO.
The major contribution of the research work is explained as follows:

- **Proposed EHSCO-based Deep Residual Network for DR detection:** An effective DR approach is devised using developed EHSCO-based Deep Residual Network classifier. Here, the Deep Residual Network classifier is utilized in order to enhance the performance in which the classifier is trained by the proposed optimization algorithm, named EHSCO technique.

The rest of the sections in the paper are organized as follows: section 2 explains the literature review and the challenges faced by different existing DR detection approaches, section 3 elaborates about the proposed EHSCO-based Deep Residual Network method, section 4describesthe results and discussion of the developed method, and the conclusion of the research work is described in section 6.

2. Motivation

In this section, some of the traditional DR detection approaches are elaborated along with their advantages and drawbacks, which motivate the researchers to devise the proposed method.

2.1 Literature Survey

The various DR detection methods are reviewed in this section. Ahsan Bin Tufail *et al.* [1] developed 3D Convolutional Neural Networks (3D CNN) for the diagnosis of DR through retinal fundus images. This method achieved superior performance in diagnosing retinal disease. However, this method failed to utilize robust data augmentation methods to work on other types of retinal diseases. Imran Qureshi *et al.* [2] introduced a multi-layer architecture of active deep learning (ADL) for detecting DR. This method effectively detected the DR-related lesions and recognized the severity levels of DR. On the other hand, this method suffers from higher computational complexities. Thippa Reddy Gadekallu*et al.* [3] devised a hybrid principal component analysis (PCA)-firefly-based deep neural network model for detecting DR in the earlier stage. The major advantage of the network model includes its capability to be implemented on the high-dimensional dataset in several other domains. Meanwhile, this performance was not observed in a low-dimensional dataset with possibilities of the method being overfitting. Grace UgochiNneji *et al.* [4] designed a weighted fusion deep learning network (WFDLN) for automatically extracting the features and for categorizing the stages of DR from fundus scans. This method works well on low-quality fundus

images. On the other hand, this method requires higher processing time to improve classification accuracy. Shaohu Wan *et al.* [5] presented Convolutional neural networks (CNNs) for detecting DR by image classification. This method improved the diagnostic efficiency but failed to minimize the overfitting issues by increasing the overall training samples. P. Saranya and S. Prabakaran [6] introduced a CNN method for the automatic identification and grading of DR using retinal fundus images. This method helped the clinical professionals to detect the disease in the earlier stage using fundus images. However, the classification efficiency depends highly on the quality of the images used. Iqra Bibi *et al.* [7] devised a DR detection method for detecting DR using fundus images. This method was computationally efficient and it effectively improved the generalization performance. On the other hand, this method failed to consider the shape characteristics of red lesions for removing the false candidates. Gayathri S *et al.* [8] devised a lightweight CNN for DR diagnosis by identifying the lesions related with disease-caused vascular anomalies. This method minimized the parameters of CNN model for facilitating real-time deployment while enhancing the accuracy of classification. However, the devised method failed to detect various types of retinal diseases.

In 2023, Nahiduzzaman *et al.* [29] have implemented an Automated detection technique using fundus images. Initially, the images were pre-processed through Contrast Limited Adaptive Histogram Equalization (CLAHE) to enhance lesions in the images. The pre-processed image was then feature extracted with fewer parameters. Then Extreme learning machine (ELM) algorithm was used for classification. Several performance metrics were then assigned and performance was analyzed to get the expected result.

In 2023, Usman *et al.* [30] have executed ML-FEC for the identification and classification of DR. Initially, Fundus Photographs were pre-processed using Principal Component Analysis (PCA). The feature was extracted through the CNN network from images. Then the subset of the images was trained through transfer learning. Further, parameters were tuned to identify different types of lesions present in each image. After that, ML-FEC was used for multi-label classification where X denotes features of the input and Y denotes five stages of DR classification from mild level to severe levels. This method helped to detect DR in the early stages. These results showed it was suitable for clinical practice and large-scale screening of patients easily.

In 2023, Chincholi, F. and Koestler, H [31] have used DNN with two pre-trained datasets. Initially, A large datasets was used, Which contained labelled examples of healthy and diseased retinae. The trained models were then used to analyse new medical imaging data by identifying regions where there may be signs of diabetic retinopathy or macular edema based on specific features like microaneurysms, cotton-wool spots, hard exudates or haemorrhages. Once detected through image segmentation methods provided by Faster RCNN/Mask RCNN algorithms, these areas were potentially be flagged for further examination by healthcare professionals who specialize in ophthalmology.

In 2023, Luo *et al.* [32] have applied DNN for the detection of DR. Initially the features were separated from the images. Where patches Bj and Qj were the subsets of the feature map. The feature from the Bj patch was taken as the weighted sum over all other patches in I. Then gaussian function was determined through wrights wo(B-I,Q_j) to find the similarities between the patches. To display the result in the screen non-local screen algorithm was used. Patch-wise relationships were then used to enhance local patch features since lesions associated with DR usually appear as plaques on fundus photographs. The Long-Range unit was incorporated into our network architecture for flexibly embedded within existing trained models without disrupting their performance. The experimental results achieved higher accuracy than existing models.

In 2023, Mondal *et al.* [33] have ensembled DL model for detection. Initially for the prediction of DR two ensembles were used. Using CLAHE method, the fundus image of retina was pre-processed for histogram equalization. Here the images were splited into high- and low-class images. The high-class images were augmented using GAN data augmentation because of its imbalance in the dataset. Then the low level was compared with proliferative types. Then the obtained data were evaluated with other data sets to evaluate the effectiveness of the method

In 2023, Vijayan, M [34] have adopted computer-assisted solution for identification of DR through CNN. Initially, the image was pre-processed to remove unwanted noise and distractions. They also enhanced the images to its appropriate pixel for its process. Then the features of the images were extracted for further process. Then regression approach was used to rate the ICDR scale continuously. Which helps in understanding the condition easily than the traditional multi-class classification. Then the images were trained through CNN models. Finally, the images were evaluated to find their accuracy and sensitivity. The result was then compared with the existing model and found that it outperformed the existing models.

In 2023, Sundaram *et.al.* [35] have tried Ensemble Convolutional Neural Network (ECNN) for DR detection. Initially, Digital colour was applied to images to differentiate blood vessels and features through Gray-Level Dependence Matrix (GLDM). Then the processed images were enhanced through

Harris Hawks Optimization. After that, the HHO algorithm was used for the classification of DR and DME through the segmentation phase. The ECNN also used to enhance the accuracy of the diagnosis performance. Finally, the performance was evaluated and the result outperformed the existing method.

In 2023, Fayyaz *et al.* [36] have presented DL for DR detection. Initially, images were pre-processed and the feature was extracted and data augmentation was applied to the images. Ant Colony systems were to choose the important attributes which were then passed through SVM with multiple kernels to get accurate results. Overall, this method provided automated detection for effective early diagnosis of DR before patients lose vision due to delayed treatment.

2.2 Challenges

The various challenges faced by existing DR detection methods are explained as follows,

- Diabetic retinopathy causes retinal damage and can lead to vision loss. Therefore, early detection of DR grade plays an important role in treatment.
- In [2], the ADL algorithm was designed for DR detection using fused features. However, the major challenge lies in employing different settings of a CNN model using the large-scale annotated datasets for the diabetic maculopathy diagnosis [2].
- PCA-Firefly-based deep learning model was introduced for detecting the DR in the earlier stage. Meanwhile, this method can be further extended by discarding noisy data in Magnetoencephalography (MEG) data assessment contributing towards enhanced prediction in healthcare [3].
- Though the developed WFDLN method achieved improved identification accuracy, the main issue it faced it that this method failed to employ novel optimization algorithms and wider sets of images for diagnosis [4].
- CNN method was devised for the automatic detection of non-proliferative DR in retinal fundus images. Moreover, the pre-processing module can be further enhanced to eliminate the noises from the dataset [6].

3. Proposed Optimization-Enabled Deep Learning for DR Detection

This section describes the developed EHSCO-based Deep Residual Network classifier for detecting the DR. This developed DR detection method mainly includes the following five phases, namely pre-processing, optic disc detection, blood vessel segmentation, feature extraction and detection. Initially, the input image acquired from the dataset is fed to the pre-processing phase to remove the noises present in the image in order to enhance the quality of the image. Here, the pre-processing is done using grayscale conversion and T2FCS [20]. After that, the optic disc detection and the blood vessel segmentation are performed using the results obtained from the pre-processing phase. The optic disc detection is performed using Sparse FCM [21]. Meanwhile, blood vessel segmentation is carried out for the pre-processed image based on morphological Top-Hat transform [26] to segment the blood vessels for further processing. Then, the feature extraction is performed from grayscale image, optic disc segmented image and blood vessel segmented image for extracting the features, such as mean, variance, entropy and kurtosis. In addition, the features, like TEXTON [25] and Walsh Hadamard Transformation are extracted from the input image. Finally, the detection process is done using Deep Residual Network [22] in such a way that the training process of detection approach is carried out using proposed EHSCO algorithm. Accordingly, the developed EHSCO method is the integration of EHO [23] and SCA [24], respectively. Fig. 1 represents the schematic view of proposed EHSCO-based Deep Residual Network for DR detection.

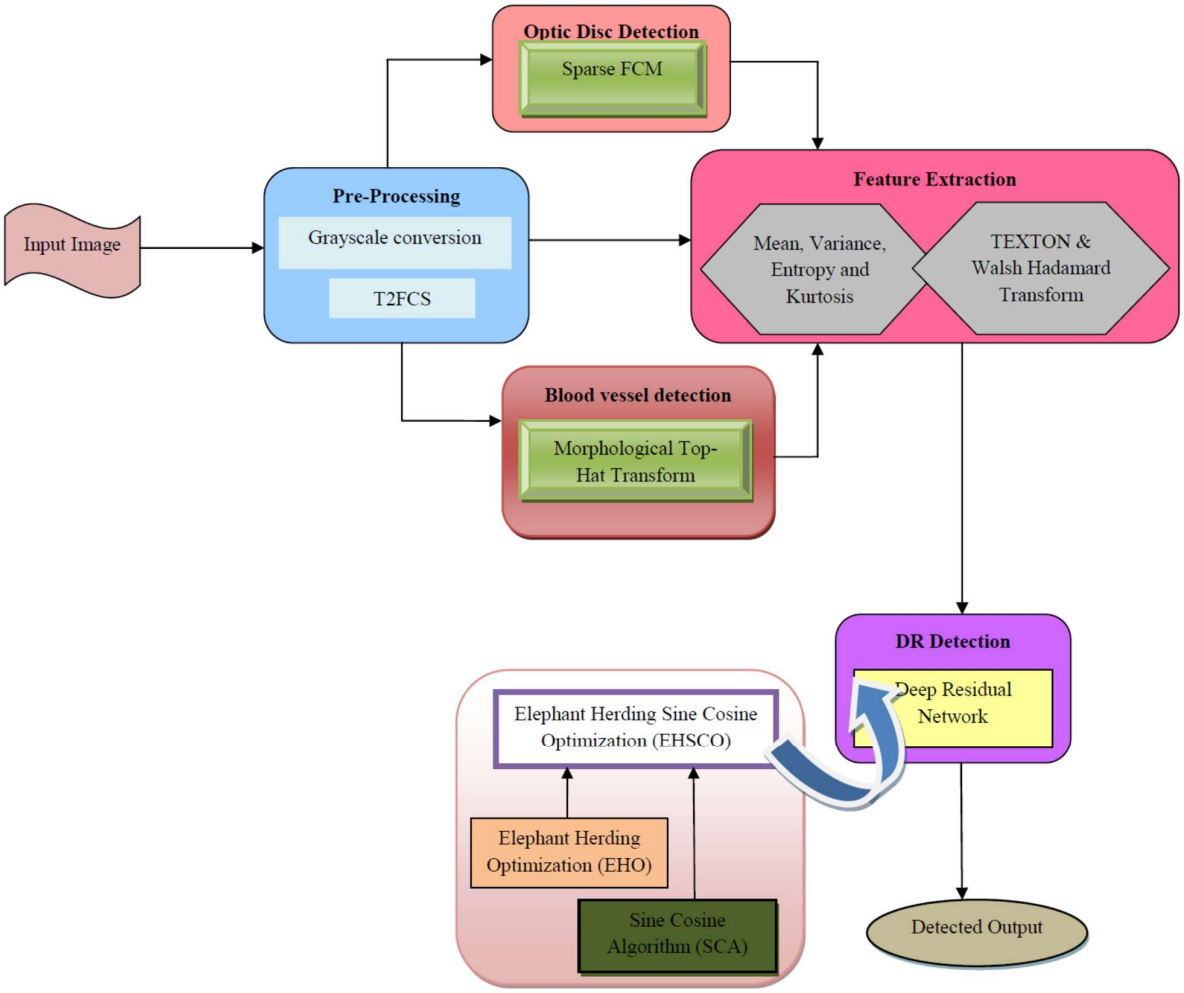

Fig1. *Block diagram of proposed EHSCO-based Deep Residual Network for DR detection*

3.1 Input Image Acquisition

Initially, the input image is acquired from the dataset. Assume a database D with h number of input images, which is given by,

$$D = \{I_1, I_2, \ldots I_r, \ldots I_h\} \quad ;1 \le r \le h \tag{1}$$

where, h represents the total number of images and I_r denotes the r^{th} image. Every image I_r is presented to the pre-processing phase.

3.2 Pre-Processing

After the acquisition of input image, pre-processing is performed for eliminating the noises or falsifications from input image. Here, the input I_r is taken as the input for pre-processing process. In this method, the input image is pre-processed based on two methods, namely Grayscale conversion and T2FCS filter to eliminate the noises from the image. The methods used for pre-processing is illustrated below as follows,

a) Grayscale conversion

The grayscale conversion technique is used to convert the color images into the shades of gray. This process removes all the color information, leaving only the luminance of each pixel.

b) T2FCS filter

T2FCS filter [20] is introduced by integrating the cuckoo search optimization method and type II fuzzy system in order to eliminate the noises in the image. Here, T2FCS filter is accomplished for pre-processing the input image. The T2FCS filter is formed by integrating Cuckoo Search (CS) optimization in type II fuzzy system wherein every member is signified based on fuzzy as 0 and 1. Besides, the type 2

fuzzy sets are adapted for keeping the image noise free without damaging the pixels present in the image. On the other hand, the degree of uncertainty is handled by type 2 fuzzy system. Therefore, T2FCS filter aid to identify the noises from corrupted image. Finally, the pre-processed output image is denoted as P^* and it is used for further processing.

3.3 Optic Disc Detection using Sparse FCM

The pre-processed image P^* is taken as an input for the optic disc detection stage for measuring the position of optic discs from input image. The optic disc detection is performed using the sparse fuzzy C-means clustering [21] for findig the discs with unique characteristics of clusters. It is shown that the accuracy of the optic disc detection relies on the appropriate clustering of the pre-processed images. The input of the sparse FCM is the image pre-processed by the gray scale conversion and T2FCS filter. The total number of images are represented as, M, and the matrix is represented as, $S_{kb} \in P^{p \times q}$. The steps of Sparse FCM to perform the optic disc detection is given below,

Step 1: Initialization: The first step is the initialization of the pre-processed weights that is signified as d, and is formulated by,

$$d = d_1^m = d_2^m = \ldots = d_p^m = \frac{1}{\sqrt{q}} \tag{2}$$

Step 2: Computation of partition matrix: For g^{th} cluster centers, and d^{th} weights of the attribute, the constrained $\alpha(K)$ that is minimizedif and only if ,

$$K_{kcc} = \begin{cases} \dfrac{1}{\Re_{cc}} & ; \quad \text{if } T_{kcc} = 0 \text{ and } \Re_{ah} = \text{card}\{b : T_{kah} = 0\} \\ 0 & ; \quad \text{if } T_{kcc} \neq 0 \text{ but } T_{k\omega} = 0 \text{ for some } \omega,\ \omega \neq cc \\ \dfrac{1}{\sum_{cc=1}^{d} \left(\dfrac{T_{kcc}}{T_{\omega cc}} \right)^{\left(\frac{1}{\delta - 1} \right)}} & ; \quad \text{Otherwise} \end{cases} \tag{3}$$

where, $\text{card}\{k : T_{kah} = 0\}$ indicates the cardinality of set $\{b : T_{kah} = 0\}$. The distance measure is represented as, T_{kcc} that signifies the distance among the k^{th} node with respect to the cc^{th} cluster center.

Step 3: Formulate the cluster centers: Assume that d and P to be fixed, and $\phi(g)$ is minimized if,

$$g_{ccb} = \begin{cases} 0 & ; \quad \text{if } d_b = 0 \\ \dfrac{\sum_{cc=1}^{d} \chi_{kcc}^{\delta} . S_{kb}}{\sum_{cc=1}^{d} \chi_{kcc}^{\delta}} & ; \quad \text{if } d_S \neq 0 \end{cases} \tag{4}$$

where, the weight component is denoted as δ to control the membership degree that is shared with the fuzzy clusters, $cc = 1,\ldots, m_0$ and $b = 1,\ldots, N$. The b^{th} feature to the objective function is represented as d_b and the term P refers the dissimilarity measure.

Step 4: Determination of class: The class is identified with respect to the fixed clusters $g = \{g_1, g_2, \ldots, g_{cc}, \ldots, g_{m_0}\}$ with the membership χ. The class E_b is computed using the objective function that is expressed as,

$$\max_{d} \sum_{b=1}^{N} d_b . E_b \text{ such that } \|d\|_2^2 \leq 1,\ \|d\|_o^o \leq \eta \text{ generates } d^*$$

where, the tuning parameter is signified as η, and $(0 \le p0 \le 1)$; $\|aa\|_o^o = \sum_{l_s=1}^{E_f} |aa_1|^o$.

Step 5: Terminate: The iteration is repeated till the iteration reaches the maximum count. The termination criterion is formulated as,

$$\frac{\sum_{b=1}^{\omega} \left| d_b^* - d_b^{\ell} \right|}{\sum_{b=1}^{N} \left| d_b^{\ell} \right|} < 10^{-4} \tag{5}$$

The discs detected with respect to the Sparse FCM is given as,

$$E_1 = I_1, I_2, ..., I_W, ..., I_{ZZ} \tag{6}$$

where, I_W indicates the w^{th} disc, and the term *zz* signifies the number of discs. The optic disc segmented output is represented as, O_d.

3.4 Blood vessel detection using Morphological Top-Hat transforms

Once the optic disc is detected, the pre-processed image P^* is taken as input for the blood vessel detection step, which is done using Morphological Top-Hat transforms. The morphological Top-hat transform [26] has been employed in the blood vessel detection operations with two sets. One set contains the image to be processed, and the other set contains the structuring element. Several morphological operations are defined based on two fundamental operations, namely, dilation and erosion.

Let e and A represents the grayscale image and structuring element. The dilation and erosion of $e(y,x)$ by $A(i,j)$ indicated by $e \oplus A$ and $e \Theta A$ are expressed as follows,

$$e \oplus A = \max_{i,j}(e(y-i, x-j) + A(i,j)) \tag{7}$$

$$e \Theta A = \min_{i,j}(e(y+i, x+j) - A(i,j)) \tag{8}$$

According to dilation and erosion, opening and closing of $e(y,x)$ by $A(i,j)$ indicated by $e \circ A$ and $e \bullet A$ are expressed as follows,

$$e \circ A = (e \Theta A) \oplus A \tag{9}$$

$$e \bullet A = (e \oplus A) \Theta A \tag{10}$$

By opening and closing the top-hat transform, including white top-hat transform and black top-hat transform, represented by WTH and BTH, are formulated as,

$$WTH(y,x) = e(y,x) - e \circ A(y,x) \tag{11}$$

$$BTH(y,x) = e \bullet A(y,x) - e(y,x) \tag{12}$$

Opening can smooth the brighter regions of the image with respect to the size of the structuring element. Hence, WTH is utilized for extracting the bright regions of the image. In the same way, closing could smooth the dim regions of the image corresponding to the size of the used structuring element. Therefore, BTH is usually used for extracting the dim regions. Finally, the blood vessel output is represented as B_d.

3.5 Feature Extraction

The feature extraction process is performed to extract the necessary features by considering the output obtained from the pre-processing phase P^*, optic disc detection phase O_d, and blood vessel detection phase B_d. The feature extraction process is significant for detecting the DR, whereas the features extracted ensures the effectiveness of DR detection. The features, like mean, variance, entropy and kurtosis are extracted from the segmented output and optic disc detected output, and pre-processed output. In addition, TEXTON features and Walsh Hadamard transform features are also extracted. The features extracted are illustrated below as follows.

a) Mean: It is a feature that extracts the mean value of the pixels present in the image, and it is formulated as,

$$Q1 = \frac{1}{|f(G1)|} \times \sum_{l=1}^{|f(G1)|} f(G1) \tag{13}$$

where, l signifies the total number of segments, $f(G1)$ denotes each segments with its value of pixel, the total number of pixels within a distribution is symbolized as $|f(G1)|$, and $Q1$ implies the mean feature.

b) Variance: Variance is a feature that effectively removes the improper features. The variance is computed using mean value and it is given by,

$$Q2 = \frac{\sum_{l=1}^{|f(G1)|} |G1 - Q1|}{f(G1)} \tag{14}$$

where, $Q2$ signifies the variance feature.

c) Entropy: The entropy of the image is computed pixel-wise, and is expressed as,

$$E(\rho Z, \rho Y) = \sum_{Z=1}^{u(\rho Z)} P(\rho Z = Z, \rho Y = Y).\log(\rho Z = Z, \rho Y = Y) \tag{15}$$

where, $E(\rho Z, \rho Y)$ denotes image pixels entropy, $u(\rho Z)$ represents exclusive pixel values, and (Z, Y) signifies pixel location of the image. The entropy feature is expressed as $Q3$.

d) Kurtosis: Kurtosis finds whether the data is peak or flat relative with respect to normal distribution.

$$Q4 = \frac{\sum_{l=0}^{n-1} (l - f1)^4 . G(l)}{(f3)^4} \tag{16}$$

where, $G(l)$ is the probability of the incidence for the individual grey level l of the image. The kurtosis feature is expressed as $Q4$.

e) Texton features: The Texton [25] features utilized for extracting the features is illustrated below. Assume there exist 2×2 grid in the image, and the image pixels are represented as V_1, V_2, V_3 and V_4. If four pixel values are same, then the pixels are generated as Texton. These five types of Texton are denoted as $T1, T2, T3, T4$ and $T5$. Here, it is moved by one pixel in every direction wherein a 2×2 grid is created. The established Texton are used for finding every grid and depict one of them forms in grid. This kind of Texton may determine a unit of Texton image and consists of five units of Texton images. In these five units of Texton image, the pixels of Texton are kept unique and other pixels are replaced by zero. Finally, the five elements of Texton images are combined for creating a final Texton image.
Assume that the pixel position is represented as $P = (x, y)$ at identical position. Every unit of Texton image poses a pixel value and these unit of Texton image includes five-pixel values, which are denoted as $W1, W2, W3, W4$ and $W5$. The final Texton image is placed in the original value in the same position if and only if five pixel values are same. If values of "0" and nonzero appear in those five pixels, the final Texton image is placed in the values of nonzero. At this point, the Texton feature is denoted as $Q5$.

f) Walsh Hadamard transforms:
The Walsh Hadamard Transform (WHT) $Q6$ is employed in feature extraction process and the main functions are performed based on the rectangular or square waves with a range of ±1. The rectangular wave varies the width of the pulse. The major benefit is that this transform includes simple computation by multiplying the pixel values by ±1 of $N\times N$ image.

$$WH(u1, v1) = \sum_{r1=0}^{O-1} \sum_{c1=0}^{O-1} I(r1, c1)(-1)^{\sum_{i-1}^{n1-1} [bi(r1)pi(n1) + bi(c1)pi(v1)]} \tag{17}$$

The WHT utilized in the images of the squared size gallery constructing $M\times M$ blocks from each of the image. The five schemas are considered as $S1, S2, S3, S4, S5$. The schemas $S2, S3$ are modified by $S2', S3'$ and is formulated as follows,

$$\varpi = \sum_{i=2}^{O^2} |c_i| - |\gamma| \tag{18}$$

$$\varpi = \frac{\sum_{i=2}^{O^2} (c_i - \gamma)}{O^2 - 1} \tag{19}$$

Every blocks of the original image are signified in the 1-D vector $(z_1, Z_2, ..z_n)$

Finally, the feature vector F is obtained by incorporating the features, such as mean, variance, entropy, kurtosis, texton and Walsh Hadamard transform and the equation is expressed by,

$$F = \{Q_1 Q_2, Q_3, Q_4, Q_5, Q_6\} \tag{20}$$

3.6. DR detection using the developed EHSCO-based Deep Residual Network

In this section, the detection of DR procedure is explained. Here, the Deep Residual Network is employed for the detection process. The architecture of Deep Residual Network and the optimization procedure employed for training the classifier is illustrated as follows.

a) Architecture of Deep Residual Network

The detection process is carried out using the Deep Residual Network classifier and the extracted feature F is fed as an input to the network. In general, Deep Residual Network includes different layers, such as linear classifier, residual blocks, convolutional layers, and average pooling layer. Fig.2 shows the structure of Deep Residual Network.

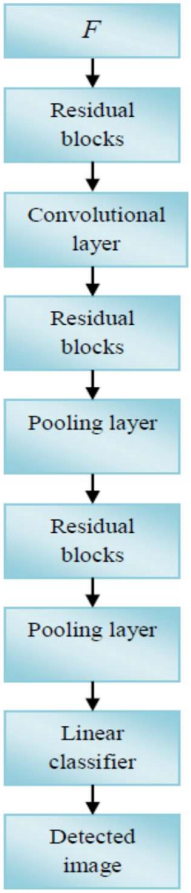

Fig.2. *Architecture of Deep Residual Network*

Convolutional (conv) layer:
The conv layer is a 2D layer that minimizes training parameters and the input image is processed using a filter sequence called the kernel. The conv layer uses a mathematical process to reduce the matrix filter of the input and then evaluate the kernel product. The computation process for the conv layer is expressed as follows:

$$C2d(N) = \sum_{a=0}^{x-1}\sum_{s=0}^{x-1} E_{a,s} \bullet N(u+a),(v+s) \tag{21}$$

$$C1d(N) = \sum_{U=0}^{D_{in}-1} E_U * N \tag{22}$$

where, N symbolizes CNN feature present in the input image, u and v symbolizes the recordings with the coordinates, E signify $x \times x$ kernel matrix, and is named as learnable parameter, u and v represents the location index of kernel matrix, E_U specifies the dimension of the kernel for U^{th} input neuron, and $*$ symbolizes the cross-correlation operator.

Pooling layer: This layer is mapped to the conv layer and is primarily used for reducing the spatial dimension of the feature maps. Hence, average pooling is chosen to work at any slice and depth of the feature maps.

$$a_{out} = \frac{a_{in} - U_a}{\lambda} + 1 \tag{23}$$

$$s_{out} = \frac{s_{in} - U_s}{\lambda} + 1 \tag{24}$$

where, a_{in} signifies input matrix width, s_{in} signifies height of input matrix, a_{out} and s_{out} defines the value of output. Moreover, U_s symbolizes height of kernel size and U_a specifies width of kernel size.

Activation function: Since the nonlinear activation function is applied to the learning of nonlinear and complex features, it is used to improve the nonlinearity of degraded features. A rectified linear unit (ReLU) is a non-linear activation function used to process images. The ReLU function is expressed as follows:

$$ReLU(N) = \begin{cases} 0 \; ; \; N < 0 \\ N \; ; \; N \geq 0 \end{cases} \tag{25}$$

Here, N denotes feature.

Batch normalization: Here, the training set is partitioned into numerous small sets called mini-batches for training the model. Here, the input layer is normalized by scaling and modifying the activation to increase the speed and consistency of training.

Residual blocks: These blocks indicate the link relationships between the conv layers. If the input and output are the same size, the input is directly connected to the output. If the sizes are different, use the dimension adjustment factor to adjust the output from the input.

$$O = J(N) + N \tag{26}$$

$$O = J(N) + R_N N \tag{27}$$

Here, N and O denotes residual blocks of input and output, J specifies mapping relationship, and R_N implies dimension matching factor.

Linear classifier: The linear classifier recognized the DR from the input image. A linear classifier is an amalgamation of a fully connected layer and as of tmax function. However, the equation is given as,

$$O = R_{i \times j} N_{l \times m} + \upsilon_{i \times m} \tag{28}$$

Here, $R_{i \times j}$ represents the weight of the matrix with $i \times j$ size, $N_{l \times m}$ denotes the input feature map with $l \times m$ dimension and υ specifies bias. Fig.3 depicts the structural view of Deep Residual Network. Here, the output is represented as D_O.

b) Training process of Deep Residual Network using EHSCO optimization algorithm
The training procedure of Deep Residual Network is done with the EHSCO optimization algorithm. Here, the weight of the classifier is trained using the developed EHSCO for achieving the optimal solution. EHSCO modifies the Deep Residual Network by integrating the EHO [23] with the SCA [24] for

selecting the optimal weights. The EHO is an algorithm based on swarm intelligence that simulates the clan updating and partitioning character of elephants. The EHO method has been effectively employed in a variety of fields for enhancing the parameter selection performance. On the other side, the SCA is a global optimization technique, which is utilized based on two trigonometric functions, such as sine function and cosine function. These functions are utilized to vary the set of candidate solutions, and the operators employed in this approach generate a balance among the exploration and exploitation of the search space in order to find the best values. The integration of EHO with the SCA reveals the efficiency of the proposed scheme and effectively improved the global search ability, and convergence speed. The algorithmic steps illustrated in the proposed EHSCO are explained as follows:

Step 1: Initialization: The primary step is the initialization of the solution Y, and it is formulated as,

$$Y = \{Y_1, Y_2, ... Y_k, ... Y_l\} \quad ; 1 \le k \le l \tag{29}$$

where, l signifies the overall solutions and Y_k represents the k^{th} solution

Step 2: Fitness function estimation: The fitness function is a measure which is employed to calculate the best optimal solution to classify the DR and it is expressed as,

$$\text{Fitness} = \frac{1}{\vartheta_S} \sum_{\beta=1}^{\vartheta_S} [T_o - D_o] \tag{30}$$

where, T_o denotes the target output, D_o specifies the classified output, and ϑ implies the total number of samples.

Step 3: Solution Update: Using the sine and cosine functions, the solution is determined by equation (31) and (32), and hence the updated equation is formulated as,

$$Y_i = Y_i^Z + t_1 \times \sin(t_2) \times \left| t_3 z_i^Z - Y_i^Z \right| \tag{31}$$

$$Y_i = Y_i^Z + t_1 \times \cos(t_2) \times \left| t_3 z_i^Z - Y_i^Z \right| \tag{32}$$

where, t_1, t_2, t_3, t_4 represents the random variables, Z_i indicates the location of the destination point in i^{th} dimension, Y_i represents the current solution, and $\left| \ \right|$ denotes the absolute value.

$$Y_i^{Z+1} = \begin{cases} Y_i^Z + t_1 \sin(t_2) \left| t_3 z_i^Z - Y_i^Z \right| & \text{if } t_4 < 0.5 \\ Y_i^Z + t_1 \cos(t_2) \left| t_3 z_i^Z - Y_i^Z \right| & \text{if } t_4 \ge 0.5 \end{cases} \tag{33}$$

$$Y_i^{Z+1} = Y_i^Z + t_1 \sin(t_2) \left| t_3 z_i^Z - Y_i^Z \right| \tag{34}$$

Assuming $z_i^Z > Y_i^Z$,

$$Y_i^{Z+1} = Y_i^Z + t_1 \sin(t_2) t_3 z_i^Z - t_1 \sin(t_2) Y_i^Z \tag{35}$$

From EHO,

$$Y_i^{Z+1} = Y_i^Z + \alpha \left(Y_{best} - Y_i^Z \right) t \tag{36}$$

$$Y_i^{Z+1} = Y_i^Z + \alpha Y_{best} t - \alpha Y_i^Z t \tag{37}$$

$$Y_{best} = \frac{Y_i^{Z+1} - Y_i^Z + \alpha Y_i^Z t}{\alpha t} \tag{38}$$

Substituting equation (38) in the target positions of SCA given in (35),

$$Y_i^{Z+1} = Y_i^Z + t_1 \sin(t_2) t_3 \left(\frac{Y_i^{Z+1} - Y_i^Z + \alpha Y_i^Z t}{\alpha t} \right) - t_1 \sin(t_2) Y_i^Z \tag{39}$$

$$Y_i^{Z+1} = Y_i^Z + \frac{t_1 \sin(t_2) t_3 Y_i^{Z+1}}{\alpha t} + t_1 \sin(t_2) t_3 \frac{\alpha Y_i^Z t - Y_i^Z}{\alpha t} - t_1 \sin(t_2) Y_i^Z \tag{40}$$

$$Y_i^{z+1} - \frac{t_1 \sin(t_2) t_3 Y_i^{z+1}}{\alpha t} = Y_i^z + t_1 \sin(t_2) Y_i^z \left(t_3 \left(\frac{\alpha t - 1}{\alpha t} \right) - 1 \right) \quad (41)$$

$$Y_i^{z+1} \left(1 - \frac{t_1 \sin(t_2) t_3}{\alpha t} \right) = Y_i^z + t_1 \sin(t_2) Y_i^z t_3 \left(t_3 \left(\frac{\alpha t - 1}{\alpha t} \right) - 1 \right) \quad (42)$$

$$Y_i^{z+1} \left(\frac{\alpha t - t_1 t_3 \sin(t_2)}{\alpha t} \right) = Y_i^z + t_1 \sin(t_2) Y_i^z \left(t_3 \left(\frac{\alpha t - 1}{\alpha t} \right) - 1 \right) \quad (43)$$

$$Y_i^{z+1} = \frac{\alpha t}{\alpha t - t_1 t_3 \sin(t_2)} \left[Y_i^z \left(1 + t_1 \sin(t_2) \left(t_3 \left(\frac{\alpha t - 1}{\alpha t} \right) - 1 \right) \right) \right] \quad (44)$$

$$Y_i^{z+1} = \begin{cases} \frac{\alpha t}{\alpha t - t_1 t_3 \sin(t_2)} \left[Y_i^z \left(1 + t_1 \sin(t_2) \left(t_3 \left(\frac{\alpha t - 1}{\alpha t} \right) - 1 \right) \right) \right] & t_4 < 0.5 \\ \frac{\alpha t}{\alpha t - t_1 t_3 \cos(t_2)} \left[Y_i^z \left(1 + t_1 \cos(t_2) \left(t_3 \left(\frac{\alpha t - 1}{\alpha t} \right) - 1 \right) \right) \right] & t_4 \geq 0.5 \end{cases} \quad (45)$$

where,

$$t_1 = w - z \frac{w}{U} \quad (46)$$

where, w represents the constant, z represents the current iteration, and U indicates the maximum number of iterations. t_1 is a random variable used to determine the area of the next solution, t_2 is a variable used for finding the distance of the movement of the next solution, which lies between $[0,2\pi]$, t_3 gives the random weights for Z_i, t_4 is used to switch among the sine and cosine functions and $r_1\alpha$ lies in the range of $[0,1]$, respectively.

Step 4: Evaluate the feasibility of the solution: In step 4, the feasibility is evaluated with the help of objective function. If the solution obtained is better than the previous solution, then it is replaced by the newly achieved solution.

Step 5: Termination: The algorithm executes the steps of optimization until the iteration reaches the best solutions. The algorithmic steps of the proposed EHSCO-Based Deep Residual Network are illustrated in algorithm 1.

Algorithm 1: Pseudo code for the developed EHSCO-based Deep Residual Network

```
Input: Y
Output:Optimal candidate solutions
Start
        Randomly initialize the population
      Compute the fitness function
Identify the best search agents
repeat
Evaluate each of the search agents based on their objective functions
Update the best solution achieved (Z=Y*)
Update t1, t2, t3 and t4
Update the position of the search agents using equation (33)
Until (t< maximum number of iterations)
Return the best solution
Replace the solution using equation (45)
End
```

4. Results and Discussion

The analysis of developed EHSCO-based Deep Residual Network technique with classical methods using DIARETDB0 and DIARETDB1 dataset is illustrated by considering the metrics, such as TPR, TNR and accuracy.

4.1 Experimental Setup

The implementation of proposed EHSCO-based Deep Residual Network technique is performed in MATLAB tool with PC having Windows 10 OS, 2GB RAM, and Intel i3 core processor.

4.2 Dataset Description

The experimentation of developed EHSCO-based Deep Residual Network approach is carried out with DIARETDB0 and DIARETDB1 dataset

4.2.1. DIARETDB0 dataset and DIARETDB1 dataset

DIARETDB0 and DIARETDB1 dataset [27] is a public database for benchmarking the DR detection from the digital images. The major aim of the database has been to explicitly characterize a database, and a testing protocol for benchmarking the DR detection methods. By employing this database and the distinct testing protocol, the results among several methods can be compared.

4.3 Performance Evaluation Measures

The efficiency of the proposed EHSCO-based Deep Residual Network technique can be analyzed by considering the TPR, TNR and accuracy metrics.

4.3.1. TPR: It is a metric which is used for measuring the severity stage of DR, and it is given by,

$$\text{Sensitivity} = \frac{{}_{t}\mathrm{p}}{{}_{t}\mathrm{p} + {}_{f}\mathrm{n}} \tag{47}$$

4.3.2. TNR: TNR is a metric, which is used for measuring the DR accurately, and it is formulated as,

$$\text{Specificity} = \frac{{}_{t}\mathrm{n}}{{}_{t}\mathrm{n} + {}_{f}\mathrm{p}} \tag{48}$$

4.3.3. Accuracy: It is a metric that defines the degree of closeness of the DR, and is expressed as,

$$\text{Accuracy} = \frac{{}_{t}\mathrm{p} + {}_{t}\mathrm{n}}{{}_{t}\mathrm{p} + {}_{f}\mathrm{p} + {}_{f}\mathrm{n} + {}_{t}\mathrm{n}} \tag{49}$$

where, t^p specifies true positive, f^p indicates false positive, t^n specifies true negative and f^n implies false negative.

4.4 Experimental Results

The experimental results of developed EHSCO-based Deep Residual Network technique for DR detection are portrayed in fig. 3. The input image is showed in fig. 3 a), and 3 b) portrays the gray scale image, Filtered image output is portrayed in fig. 3 c) and 3d) shows the output of optic disc detected image and the segmented image is signified in fig. 3 e).

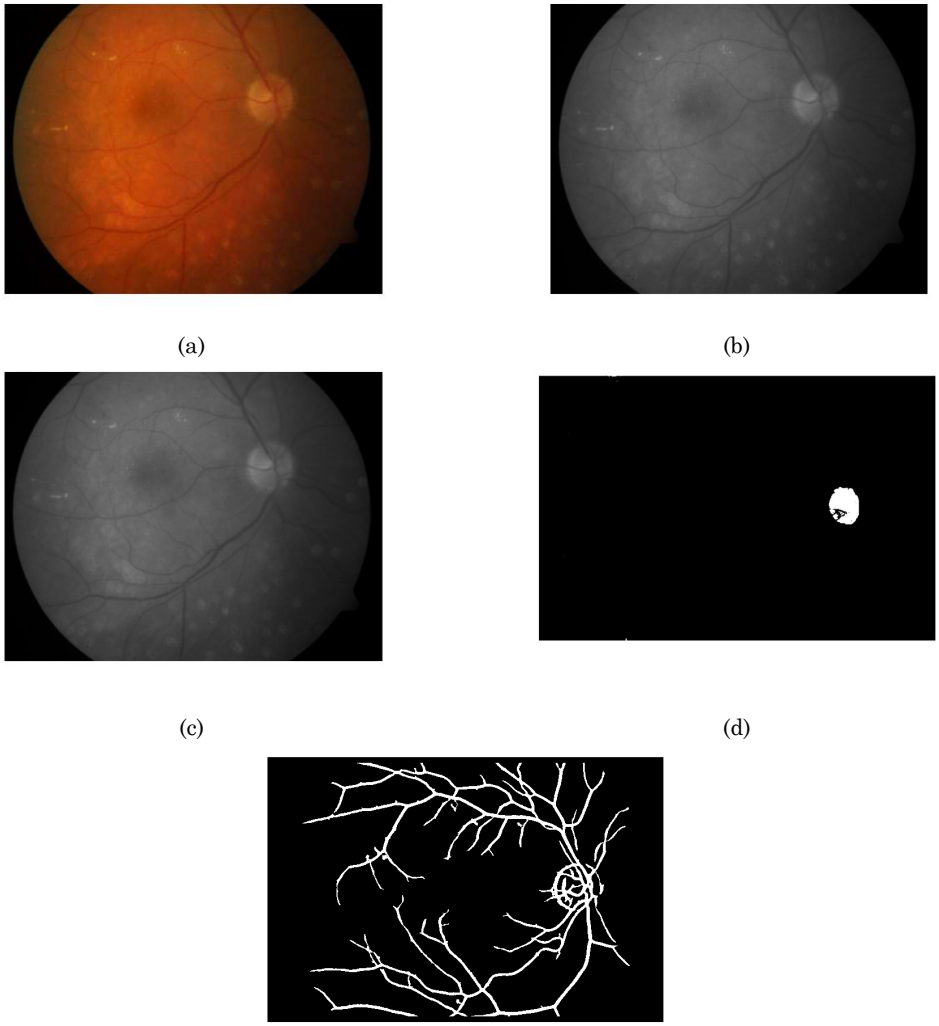

(a) (b)

(c) (d)

(e)

Fig.3. *Experimental results of proposed EHSCO-based Deep Residual Network a) Input images b) Pre-processed image output by gray scale conversion c) Pre-processed image output by T2FCS filter d) output of optic disc detected image using Sparse FCM e) Segmented image output*

4.5 Performance Analysis

The performance analysis of the developed EHSCO-based Deep Residual Network algorithm with respect to TPR, TNR and accuracy parameters is computed by varying the training data percentage.

4.5.1 Analysis using Training Data based on DIARETDB0 Dataset

The performance analysis of developed EHSCO-based Deep Residual Network with epoch by varying training data percentage based on TPR, TNR and accuracy is displayed in fig. 4. Fig. 4a) portrays the TPR analysis with epoch by varying the training data percentage. By considering the 70% training data, the TPR value obtained by the EHSCO-based Deep Residual Network for the epoch 20 is 0.829, epoch 40 is 0.864, epoch 60 is 0.871, and the epoch 80 is 0.933. The performance analysis of the TNR metric by considering the training data percentage is shown in fig. 4b). In 50% of training data, the developed EHSCO-based Deep Residual Network technique obtained a TNR value of 0.791 for epoch 20, 0.814 for epoch 40, 0.814 for epoch 60, and 0.892 for epoch 80. Fig. 4c) presents the performance analysis of accuracy by varying the training data percentage. The accuracy value achieved by the developed EHSCO-based Deep Residual Network for the epoch 20, 40, 60, and 80 is 0.855, 0.871, 0.885, and 0.936 for 80% of training data.

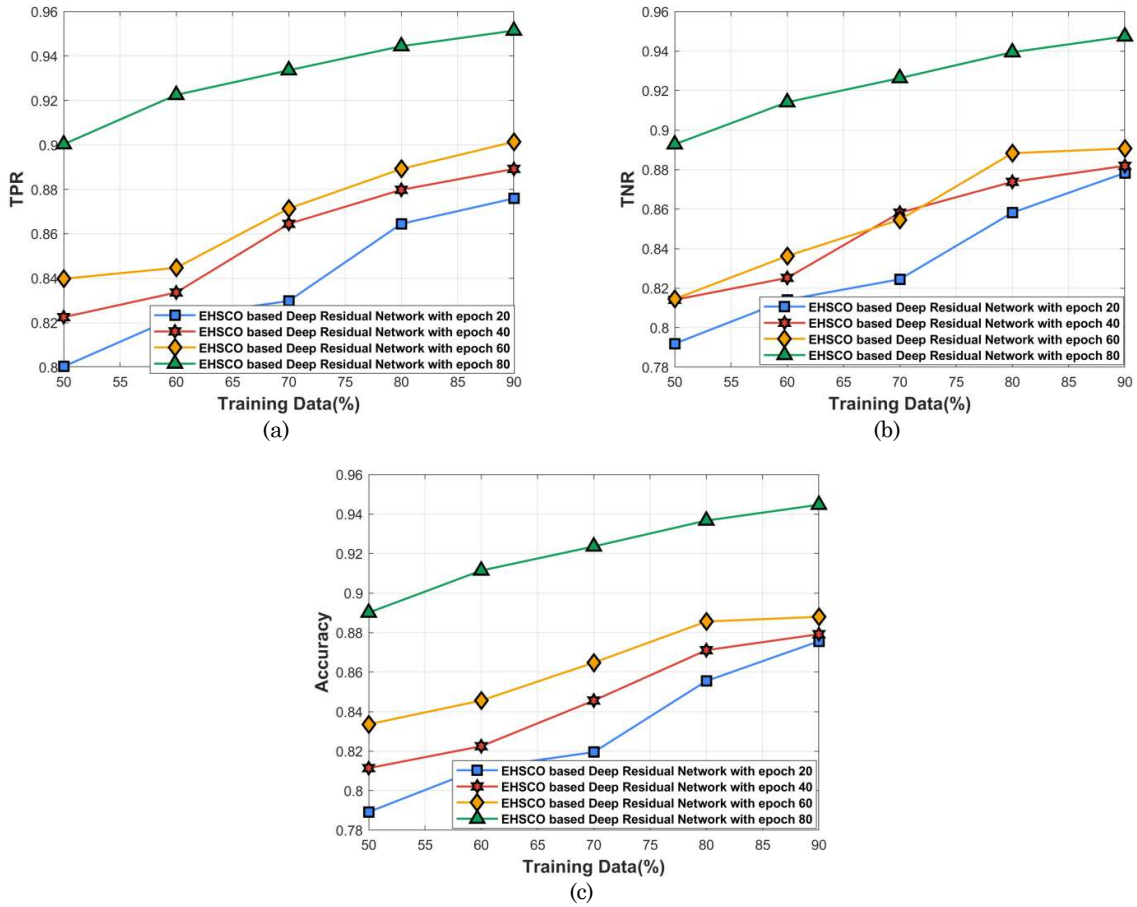

Fig.4. *Performance analysis of methods with DIARETDB0 dataset considering training data with a) TPR b) TNR c) Accuracy*

4.5.2 Analysis using Training Data based on DIARETDB1 Dataset

In fig. 5, the performance analysis of developed EHSCO-based Deep Residual Network with epoch 20, 40, 60, and 80 based on TPR, TNR and accuracy by varying the training data is displayed. The analysis of TPR by varying the epoch is shown in fig. 5a). The TPR achieved by the developed EHSCO-based Deep Residual Network with epoch 20, 40, 60, and 80 is 0.842, 0.863, 0.867, and 0.922 for 80% of training data. The analysis of TNR with epoch is illustrated in fig. 5 b). In 70% of training data, the developed EHSCO-based Deep Residual Network technique achieved 0.843, 0.854, 0.863, and 0.922 of TNR for epoch 20, 40, 60, and 80. Fig. 5 c) presents the performance analysis of accuracy by changing the training data percentage with respect to epoch. The developed EHSCO-based Deep Residual Network method achieved an accuracy value for epoch 20, 40, 60, and 80 is 0.798, 0.809 and 0.820, and 0.898 for the 60% of training data.

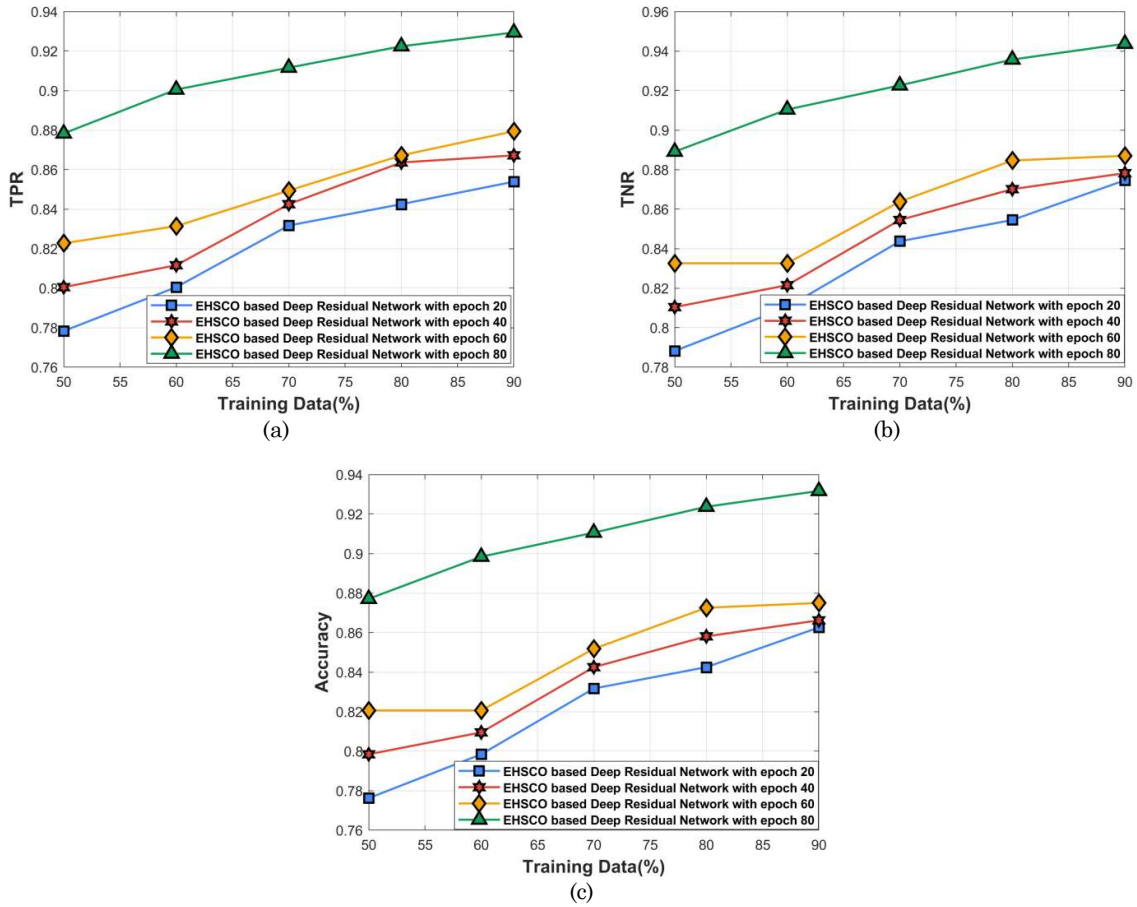

Fig.5. *Performance analysis of methods using DIARETDB1 dataset with respect to training data with a) TPR b) TNR c) Accuracy*

4.6 Comparative Techniques

The techniques taken for analysis are Deep CNN [5], Auto encoder [28], CNN [6], and proposed EHSCO-based Deep Residual Network.

4.7 Comparative Analysis

The comparative analysis of the proposed EHSCO-based Deep Residual Network algorithm based on the TPR, TNR and accuracy parameters by varying the training data percentage are computed.

4.7.1 Analysis using Training Data based on DIARETDB0 Dataset

The assessment of methods with DIARETDB0 dataset is depicted in fig. 6). In fig. 6a), the analysis of the methods with TPR is depicted. For 50% training data, the TPR measured by Deep CNN, Auto encoder, CNN and proposed EHSCO-based Deep Residual Network are 0.812, 0.834, 0.856, and 0.912. The performance improvement gained by the proposed method with respect to the existing approaches is, 10.96%, 8.527%, and 6.094%. The analysis of the methods using TNR is depicted in fig. 6b). For 50% training data, the TNR measured by Deep CNN is 0.804, Auto encoder is 0.826, CNN is 0.848, and proposed EHSCO-based Deep Residual Network is 0.905. The performance improvement achieved by the developed EHSCO-based deep residual network in comparison with the existing approaches is, 11.14%, 8.694%, and 6.241%. The assessment of techniques based on accuracy is illustrated in fig. 6c). By considering the training data as 50%, the accuracy value computed by Deep CNN, Auto encoder, CNN, and proposed EHSCO-based Deep Residual Network are 0.801, 0.823, 0.845, and 0.902. The performance improvement obtained by the developed EHSCO-based Deep Residual Network method with respect to the existing approaches is, 11.18%, 8.72%, and 6.263%.

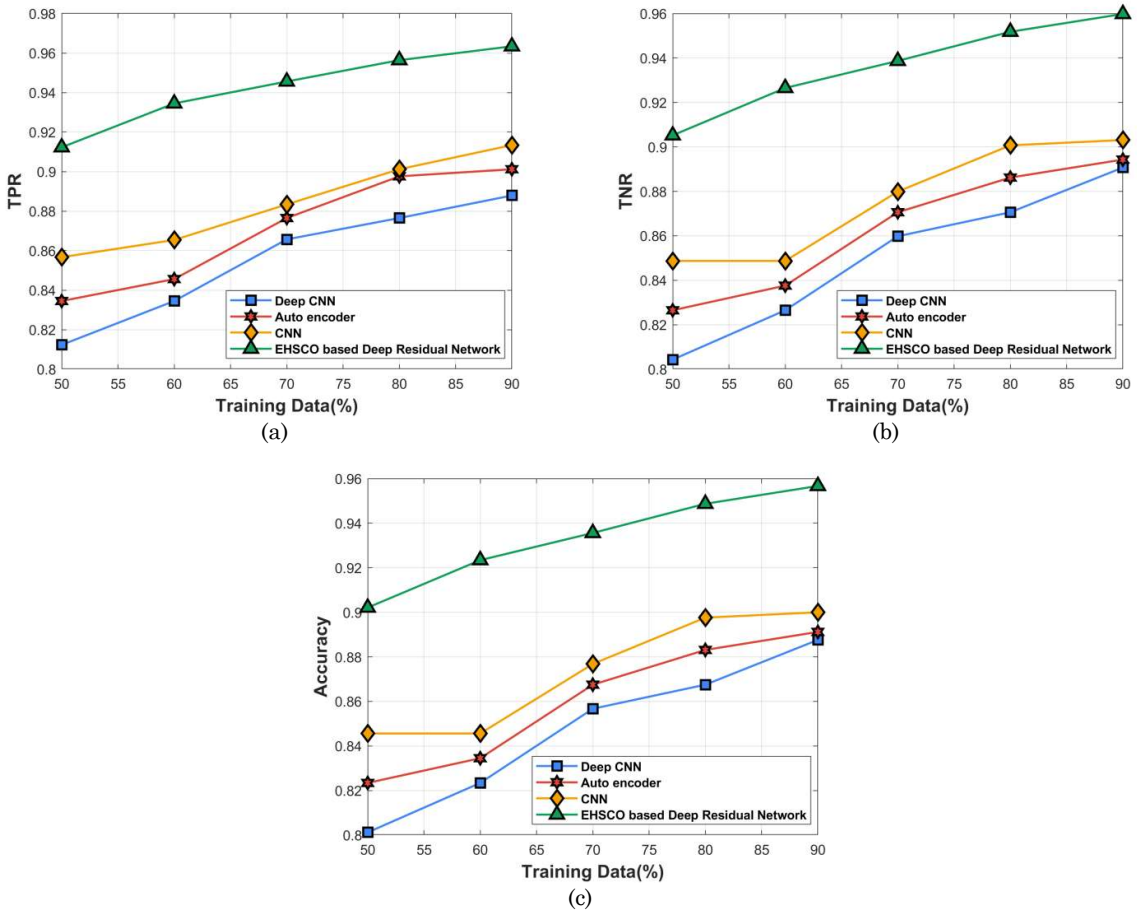

Fig.6. *Comparative analysis of methods using DIARETDB0 dataset based on the training data with a) TPR b) TNR c) Accuracy*

4.7.2 Analysis using Training Data based on DIARETDB1 Dataset

Fig. 7 illustrates the analysis of the method by considering the training data using DIARETDB1 dataset. The analysis carried out with respect to TPR is depicted in fig. 7a). When training data is 60%, TPR measured by the existing Deep CNN, Auto encoder, and CNN is 0.815, 0.826, and 0.846, whereas the proposed EHSCO-based Deep Residual Network method achieved the TPR of 0.915, respectively. The performance improvement of the proposed method while comparing with the existing Deep CNN is 10.92%, Auto encoder is 9.710%, and CNN is 7.547%, respectively. Fig. 7b) portrays the analysis of TNR measure. For the 60% training data, the TNR achieved by Deep CNN is 0.825, Auto encoder is 0.836, CNN is 0.847, and proposed EHSCO-based Deep Residual Network is 0.925, respectively. The performance gain achieved by the developed method is 10.80%, 9.606%, 8.407%with respect to the existing approaches. The analysis of accuracy by changing the training data is depicted in fig. 7c). When training data is 60%, the accuracy measured by Deep CNN, Auto encoder, CNN and proposed EHSCO-based Deep Residual Network is 0.813, 0.824, 0.835, and 0.913 respectively. The performance improvement achieved by the proposed EHSCO-based Deep Residual Network method while comparing with the existing Deep CNN is 10.94%, Auto encoder is 9.732%, and CNN is 8.517%, respectively.

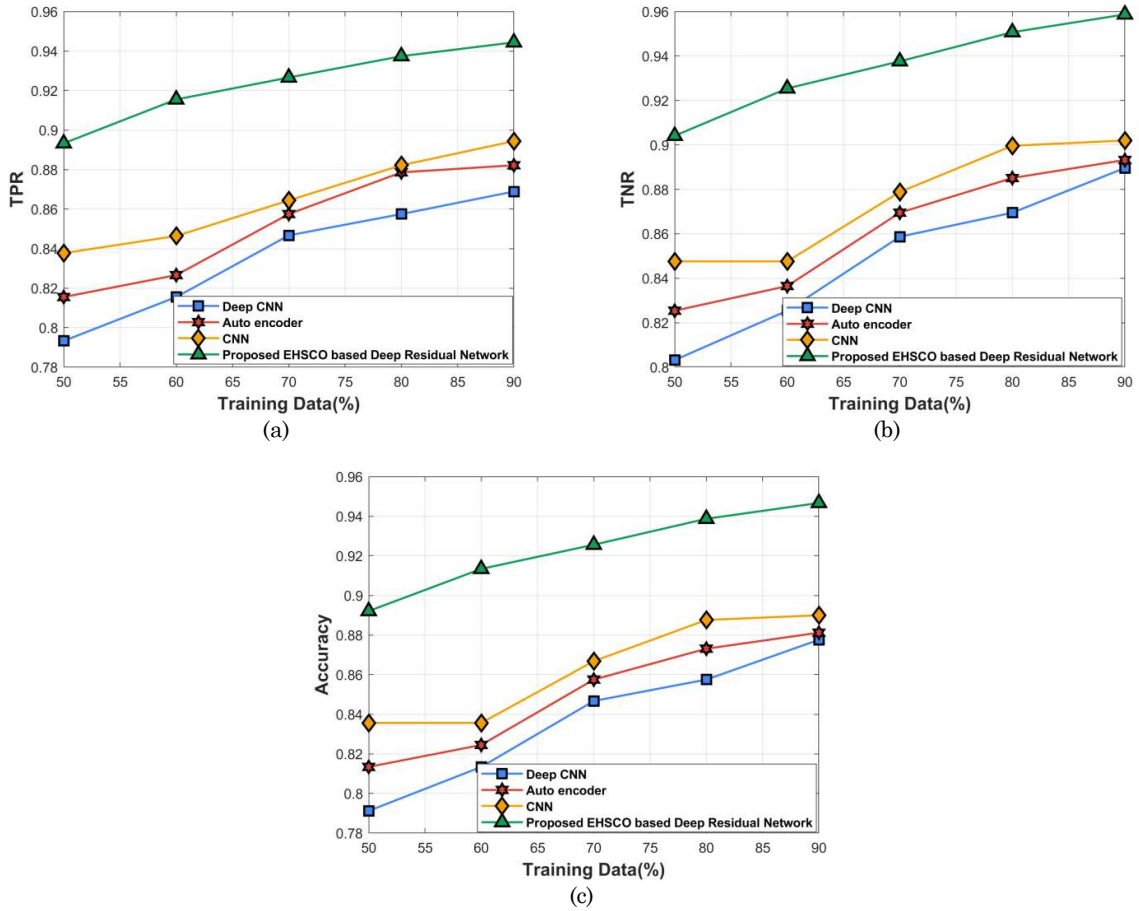

Fig.7. *Comparative analysis of methods using DIARETDB1 dataset based on the training data with a) TPR b) TNR c) Accuracy*

4.8 Comparative Discussion

Table 1 presents the assessment of methods considering DIARETDB0 and DIARETDB1 dataset. Using DIARETDB0, the highest TPR of 0.963 is computed by proposed EHSCO-based Deep Residual Network, while the TPR measured by Deep CNN, Auto encoder and CNN are 0.887, 0.901, and 0.913.The highest TNR of 0.959 is computed by proposed EHSCO-based Deep Residual Network while the TNR measured by Deep CNN, Auto encoder and CNN are 0.890, 0.894, and 0.903. The highest accuracy of 0.956 is computed by developed EHSCO-based Deep Residual Network while the accuracy measured by Deep CNN, Auto encoder and CNN are 0.887, 0.891, and 0.9. Using DIARETDB1, the highest TPR of 0.944, and highest TNR of 0.957 and highest accuracy of 0.946 is computed by developed EHSCO-based Deep Residual Network. From the discussion, it is clearly shown that the developed EHSCO-based Deep Residual Network obtained a higher TPR of 0.963, higher TNR of 0.959, and higher accuracy of 0.956, respectively.

Table 1: Comparative Analysis

Dataset		Metrics	Deep CNN	Auto encoder	CNN	Proposed EHSCO-based Deep Residual Network
DIARETDB0	*Training data%=90*	TPR	0.887	0.901	0.913	0.963
		TNR	0.890	0.894	0.903	0.959
		Accuracy	0.887	0.891	0.9	0.956
DIARETDB1	*Training data%=90*	TPR	0.868	0.882	0.894	0.944
		TNR	0.889	0.893	0.902	0.958
		Accuracy	0.877	0.881	0.89	0.946

5. Conclusion

A robust and efficient detection approach is developed to detect the DR using the proposed EHSCO optimization algorithm. At first, the input image is fed to the pre-processing phase in order to eliminate the noises from the input image. After that, the pre-processed image is subjected to the object disc detection phase, and the blood vessel segmentation phase. The results obtained from this step is presented to the feature extraction phase to extract the required features, such as TEXTON, Walsh Hadamard transform, mean, variance, entropy and kurtosis for further processing. Thereafter, the features selected are subjected to the final phase, called DR Detection Phase, which is carried out using the Deep Residual Network classifier, whereas the Deep Residual Network classifier is trained by the developed EHSCO optimization algorithm. EHSCO algorithm is an integration of EHO and SCA, respectively. However, the performance of the developed EHSCO optimization algorithm is evaluated using the performance metrics, such as, TPR, TNR and accuracy, and achieved the higher TPR of 0.963, higher TNR of 0.959, and maximal accuracy of 0.956 using DIARETDB0 dataset. The future dimension of this research work would be the concern of designing other novel classifiers for enhancing the effectiveness of the detection performance. Furthermore, the training procedure can be processed by introducing other novel optimization algorithm for better results.

Compliance with Ethical Standards

Conflicts of interest: Authors declared that they have no conflict of interest.

Human participants: The conducted research follows ethical standards and the authors ensured that they have not conducted any studies with human participants or animals.

References

[1] Tufail AB, Ullah I, Khan WU, Asif M, Ahmad I, Ma YK, Khan R, Ali M., "Diagnosis of Diabetic Retinopathy through Retinal Fundus Images and 3D Convolutional Neural Networks with Limited Number of Samples", Wireless Communications and Mobile Computing, November 2021.

[2] Qureshi I, Ma J, Abbas Q., "Diabetic retinopathy detection and stage classification in eye fundus images using active deep learning", Multimedia Tools and Applications, vol.80, no.8, pp.11691-721, March 2021.

[3] Gadekallu TR, Khare N, Bhattacharya S, Singh S, Maddikunta PK, Ra IH, Alazab M., "Early detection of diabetic retinopathy using PCA-firefly based deep learning model", Electronics, vol.9, no.2, pp.274, February 2020.

[4] Nneji GU, Cai J, Deng J, Monday HN, Hossin MA, Nahar S., "Identification of Diabetic Retinopathy Using Weighted Fusion Deep Learning Based on Dual-Channel Fundus Scans", Diagnostics, vol.12, no.2, pp.540, February 2022.

[5] Wan S, Liang Y, Zhang Y, "Deep convolutional neural networks for diabetic retinopathy detection by image classification", Computers & Electrical Engineering, vol.72, pp.274-82, November 2018.

[6] Saranya P and Prabakaran S, "Automatic detection of non-proliferative diabetic retinopathy in retinal fundus images using convolution neural network", Journal of Ambient Intelligence and Humanized Computing, vol.15, pp.1-0, September 2020.

[7] Bibi I, Mir J, Raja G, "Automated detection of diabetic retinopathy in fundus images using fused features", Physical and Engineering Sciences in Medicine, vol.21, pp.1-2, September 2020.

[8] Gayathri S, Gopi V P, Palanisamy P, "A lightweight CNN for Diabetic Retinopathy classification from fundus images", Biomedical Signal Processing and Control, vol.62, pp.102115, September 2020.

[9] Musleh, S.; Alam, T.; Bouzerdoum, A.; Belhaouari, S.B.; Baali, H., "Identification of potential risk factors of diabetes for the qatari population", In Proceedings of the 2020 IEEE International Conference on Informatics, IoT, and Enabling Technologies (ICIoT), vol.2-5, pp. 243-246, February 2020.

[10] Nneji, G.U.; Cai, J.; Deng, J.; Monday, H.N.; James, E.C.; Ukwuoma, C.C., "Multi-Channel Based Image Processing Scheme for Pneumonia Identification", Diagnostics, vol.12, no.325, 2022.

[11] Li, J.P.; Nneji, G.U.; James, E.C.; Leta, Y.B.; Nahar, S.; Haq, A.U., "Shared Weighted Continuous Wavelet Capsule Network for Electrocardiogram Biometric Identification", In Proceedings of the 2021 18th International Computer Conference on Wavelet Active Media Technology and Information Processing (ICCWAMTIP), pp.419-425, December 2021.

[12] Nneji, G.U.; Cai, J.; Deng, J.; Nahar, S.; Mgbejime, G.T.; James, E.C.; Woldeyes, S.K., "A Dual Weighted Shared Capsule Network for Diabetic Retinopathy Fundus Classification", In Proceedings of the 2021 International Conference on High Performance Big Data and Intelligent Systems (HPBD&IS), vol.5-7, pp.297-302, December 2021.

[13] Ahmad MS, Mir J, Ullah MO, Shahid ML, Syed MA., "An efficient heart murmur recognition and cardiovascular disorders classification system", Australasian physical & engineering sciences in medicine, vol.42, no.3, pp.733-43, September 2019.

[14] Shaukat F, Javed K, Raja G, Mir J, Shahid ML., "Automatic lung nodule detection in CT images using convolutional neural networks", IEICE Transactions on Fundamentals of Electronics, Communications and Computer Sciences, vol.102, no.10, pp.1364-73, October 2019.

[15] Cheloni R, Gandolfi SA, Signorelli C, Odone A., "Global prevalence of diabetic retinopathy: protocol for a systematic review and meta-analysis", vol.9, no.3, pp.e022188, March 2019.

[16] American Diabetes Association., "11.Microvascular complications and foot care: standards of medical care in diabetes-2019", Diabetes Care, vol.42, pp.S124-38, January 2019.

[17] World Health Organization, "WHO global report on traditional and complementary medicine 2019", may 2019.

[18] Seoud L, Hurtut T, Chelbi J, Cheriet F, Langlois JP., "Red lesion detection using dynamic shape features for diabetic retinopathy screening", IEEE transactions on medical imaging, vol.35, no.4, pp.1116-26, December 2015.

[19] Qureshi I, Ma J, Abbas Q., "Recent development on detection methods for the diagnosis of diabetic retinopathy", Symmetry, vol.11, no.6, pp.749, June 2019.

[20] Kumar S V and Nagaraju C, "T2FCS filter: Type 2 fuzzy and cuckoo search-based filter design for image restoration", Journal of Visual Communication and Image Representation, vol.58, pp.619-41, January 2019.

[21] Chang X, Wang Q, Liu Y, Wang Y, "Sparse Regularization in Fuzzy C-Means for High-Dimensional Data Clustering", IEEE transactions on cybernetics, vol.47, no.9, pp.2616-27, December 2016.

[22] Chen Z, Chen Y, Wu L, Cheng S, Lin P, "Deep residual network based fault detection and diagnosis of photovoltaic arrays using current-voltage curves and ambient conditions", Energy Conversion and Management, vol.198, pp.111793, October 2019.

[23] Wang GG, Deb S, Coelho L D, "Elephant herding optimization", In proceedings of 2015 3rd International Symposium on Computational and Business Intelligence (ISCBI), pp.1-5, December 2015.

[24] Mirjalili S, "SCA: a sine cosine algorithm for solving optimization problems", Knowledge-based systems, vol.96, pp.120-33, March 2016.

[25] Leung, T. and Malik, J., "Representing and recognizing the visual appearance of materials using three-dimensional textons", International journal of computer vision, vol.43, no.1, pp.29-44, 2001.

[26] Bai, X., Zhou, F. and Xue, B., "Image enhancement using multi scale image features extracted by top-hat transform", Optics & Laser Technology, vol.44, no.2, pp.328-336, 2012.

[27] Standard DR database DIARETDB0 and DIARETDB1 taken from, "https://www.it.lut.fi/project/imageret/diaretdb0/", accessed on November 2020.

[28] Pathirage, C.S.N., Li, J., Li, L., Hao, H., Liu, W. and Ni, P., "Structural damage identification based on autoencoder neural networks and deep learning", Engineering structures, vol.172, pp.13-28, 2018.

[29] Nahiduzzaman, M., Islam, M.R., Goni, M.O.F., Anower, M.S., Ahsan, M., Haider, J. and Kowalski, M., "Diabetic Retinopathy Identification Using Parallel Convolutional Neural Network Based Feature Extractor and ELM Classifier", *Expert Systems with Applications*, pp.119557, 2023.

[30] Usman, T.M., Saheed, Y.K., Ignace, D. and Nsang, A., "Diabetic Retinopathy Detection using Principal Component Analysis Multi-Label Feature Extraction and Classification", International Journal of Cognitive Computing in Engineering, 2023.

[31] Chincholi, F. and Koestler, H., "Detectron2 for Lesion Detection in Diabetic Retinopathy", Algorithms, Vol. 16(3), pp.147, 2023.

[32] Luo, X., Wang, W., Xu, Y., Lai, Z., Jin, X., Zhang, B. and Zhang, D., "A deep convolutional neural network for diabetic retinopathy detection via mining local and long-range dependence", CAAI Transactions on Intelligence Technology, 2023.

[33] Mondal, S.S., Mandal, N., Singh, K.K., Singh, A. and Izonin, I., "EDLDR: An Ensemble Deep Learning Technique for Detection and Classification of Diabetic Retinopathy", Diagnostics, Vol. 13(1), pp.124, 2023.

[34] Vijayan, M., "A Regression-Based Approach to Diabetic Retinopathy Diagnosis Using Efficientnet", Diagnostics, Vol. 13(4), pp.774, 2023.

[35] Sundaram, S., Selvamani, M., Raju, S.K., Ramaswamy, S., Islam, S., Cha, J.H., Almujally, N.A. and Elaraby, A., "Diabetic Retinopathy and Diabetic Macular Edema Detection Using Ensemble Based Convolutional Neural Networks", Diagnostics, Vol. 13(5), pp.1001, 2023.

[36] Fayyaz, A.M., Sharif, M.I., Azam, S., Karim, A. and El-Den, J., "Analysis of Diabetic Retinopathy (DR) Based on the Deep Learning. Information", Vol. 14(1), pp.30, 2023.